View metadata, citation and similar papers at core.ac.uk
brought to you by CORE
provided by Institutional Repository of the Freie Universität Berlin

BIOLOGICAL SCIENCES: Biophysics and Computational Biology

A pH-sensitive vibrational probe reveals a cytoplasmic protonated cluster in bacteriorhodopsin

Short title: A second protonated cluster in Bacteriorhodopsin

Victor A. Lorenz-Fonfria[a,b,c,1], Mattia Saita[a], Tzvetana Lazarova[d], Ramona Schlesinger[e], and Joachim Heberle[a]

[a]Experimental Molecular Biophysics, Dept. of Physics, Freie Universität Berlin, Arnimallee 14, 14195 Berlin, Germany; [b]Institute of Molecular Science (ICMol), Universitat de València, Catedràtic José Beltrán Martínez 2, 46980 Paterna, Spain; [c]Dept. of Biochemistry and Molecular Biology, Universitat de València, Carrer Doctor Moliner 50, 46100 Burjassot, Spain; [d]Unitat de Biofísica, Departament de Bioquímica i de Biologia Molecular, and Centre d'Estudis en Biofísica, Universitat Autònoma de Barcelona, Barcelona, Spain; [e]Genetic Biophysics, Dept. of Physics, Freie Universität Berlin, Arnimallee 14, 14195 Berlin, Germany

[1]To whom correspondence should be addressed. e-mail: victor.lorenz@uv.es

Abstract. Infrared spectroscopy has been used in the past to probe the dynamics of internal proton transfer reactions taking place during the functional mechanism of proteins, but has remained mostly silent to protonation changes in the aqueous medium. Here, by selectively monitoring vibrational changes of buffer molecules with a temporal resolution of 6 µs, we have traced proton release and uptake events in the light-driven proton-pump bacteriorhodopsin and correlate these to other molecular processes within the protein. We demonstrate that two distinct chemical entities contribute to the temporal evolution and spectral shape of the *continuum* band, an unusually broad band extending from 2300 to well below 1700 cm^{-1}. The first contribution corresponds to deprotonation of the proton release complex (PRC), a complex in the extracellular domain of bacteriorhodopsin where an excess proton is shared by a cluster of internal water molecules and/or ionic E194/E204 carboxylic groups. We assign the second component of the *continuum* band to the proton uptake complex (PUC), a cluster with an excess proton reminiscent to the PRC but located in the cytoplasmic domain and possibly stabilized by D38. Our findings refine the current interpretation of the *continuum* band, and call for a reevaluation of the last proton transfer steps in bacteriorhodopsin.

Keywords. time-resolved infrared spectroscopy; proton release and uptake, protonated water clusters; proton pumping; *continuum* band

Significance Statement. The vectorial transport of protons across membranes by pumps is central to cellular bioenergetics. A persistent problem in their study is the technical unfeasibility to simultaneously resolve the dynamics of all the relevant proton transfer steps by the same method, i.e., those within the protein as well as those involving protonation changes of the aqueous medium, currently relying on complementary methods to map both. Here, we solved this limitation and monitored both internal and external protonation changes during the proton-pump mechanism of bacteriorhodopsin by time-resolved infrared spectroscopy. Our findings reveal inconsistencies with the proton uptake mechanism accepted for the last 25 years, highlighting the need of simultaneous and comprehensive monitoring protonation changes to resolve the molecular mechanism of ion pumps.

\body

Proton transfers are one of the most ubiquitous chemical reactions in living organisms. Central to cellular bioenergetics are vectorial proton transfer reactions, conducted by light- and redox-driven proton pumping membrane proteins (1, 2). Among the techniques sensitive to the protonation state of chemical groups in proteins, infrared (IR) difference spectroscopy is well-suited for tracing intra-protein proton transfer reactions due to its intrinsic high temporal resolution, straightforward applicability to membrane proteins, and exquisite sensitivity (3-7). However, IR difference spectroscopy has not yet been able to monitor the dynamics of proton release from proteins into the surrounding aqueous phase, resulting in the need of complementary techniques to provide a comprehensive picture of vectorial proton transport.

Protonation changes in the surrounding aqueous medium have been mostly probed in the visible range using pH-indicating dyes. These experiments require diluted and very weakly buffered protein solutions (8-11), in contrast to the well-buffered and highly concentrated samples used in IR spectroscopy (4, 12). It was soon realized that under low concentration of mobile buffers the released protons remain temporally trapped along the membrane surface, being detected by dye molecules in the bulk phase with a delay of ~0.5-1 ms (8, 9, 13, 14). Dyes covalently attached to the protein surface do show a fast response to proton release (10, 15-17), but complications arise because covalently attached dyes respond also to polarity changes at the protein surface (10, 15). Furthermore, their response time may depend on the distance to the proton release site (16, 17). Kinetic differences for proton detection have been observed even for dyes covalently bound to neighboring sites (15). As a final drawback, proton release/uptake kinetics may be altered whenever genetic engineering is needed to introduce a site for selective labeling (15, 17).

It is known for more than 30 years that mobile buffer molecules accelerate the migration of protons from the surface to the bulk phase (9, 14) by collisional proton transfer (18, 19). Their chemical functionality as "proton shuttles" renders buffer molecules ideal probes for detecting proton release/uptake events by vibrational spectroscopy. A further advantage of buffer molecules over pH-indicating dyes is their high solubility and compatibility with biological samples at even molar concentrations, especially for the so-called Good's buffers (20). A high buffer concentration ensures a well-controlled pH value during the entire length of the experiment and, more importantly, a fast response of the buffer to pH changes (e.g., proton release/uptake from proteins). As a drawback, extinction coefficients are typically 100 times smaller in the IR than in the visible range, which makes the use of buffer molecules as pH-sensitive probes technically more challenging than of pH-sensitive dyes.

Berthomieu and Hienerwadel reported on the use of buffer molecules to detect light-induced release of protons from photosystem II under steady-state conditions by FT-IR difference spectroscopy (21). Experiments at the same pH using two different buffer molecules (e.g., phosphate *vs* Tris buffer) were used to cancel overlapping protein contributions and to resolve buffer-only spectral changes (21). This methodology was recently improved by performing experiments with

natural and perdeuterated buffer molecules (22, 23). Further examples in the literature on the use of buffers as vibrational pH probes are scarce (21-26), and in all cases limited to steady-state experiments, unable of providing information on protonation dynamics.

A relevant example to test the potential of buffer molecules to probe the dynamics of proton release and uptake events is the light-driven proton-pump bacteriorhodopsin, BR (27). This well-known transmembrane protein powers halophilic archaebacteria under low oxygen tension (28). Its photocyclic reaction, triggered by photoisomerization of the retinal from all-*trans* to 13-*cis*, comprises a series of quasi-stable states, denoted as K, L, M, N and O intermediates (29, 30), whose interconversion and decay to the initial dark state is, under most experimental conditions (30, 31), adequately described by a sequential model including back-reactions (Fig. 1a). Compelling evidence has been presented for the existence of at least two M (32, 33) and two N intermediates (34, 35).

Specific molecular events occur during the transition between intermediates (7, 36), such as proton transfer reactions (Fig. 1a,b). The widely accepted proton pumping mechanism of BR involves a minimum of five proton transfer reactions (Fig. 1b), leading to the net transport of one proton from the CP to the EC side per photocycle (7, 37).

Gerwert and coworkers showed that the PRC, the elusive group releasing a proton to the EC medium (Fig. 1b), was characterized by an unusually broad band extending from ~2300 cm^{-1} to well below 1700 cm^{-1} (Fig. 1c), known as the *continuum* band (38, 39). This broadband feature was assigned to a protonated water cluster (39) or, more generally speaking, to a local area network (LAN) of H-bonded internal water molecules sharing an excess proton (40, 41). Indeed, similar *continua* in the 2300-1700 cm^{-1} region are predicted and observed when an excess proton is shared by a cluster of water molecules (42-44). However, a LAN where a proton is shared by the ionic side chains of E194 and E204 can also reproduce the *continuum* band (45), leading to a still open dispute about the precise chemical nature of the PRC (46). As a recent twist, Gerwert and coworkers proposed that E194 is the actual terminal proton release group (47). If correct, the rise of the *continuum* band should precede the release of protons to the EC surface, a prediction that remains untested.

Late intermediates in the photocycle of BR (from M to O, see Fig. 1a) decay in an equilibrated mixture to the initial dark state (31, 48), a situation that considerably complicates studying late proton transfer events and, consequently, the proton uptake process. Established already in 1975 (49, 50), proton uptake was initially assigned either to the decay of the M or to the decay of the O intermediate (9, 51). Fifteen years later it was reassigned to the N-to-O transition when it was shown that D96 reprotonates in the N-to-O transition in a pH-dependent manner (35, 52, 53). Later results indicated that the reprotonation of D96 from the external medium might be assisted by several charged residues at the CP surface acting as a proton antenna (54, 55) with a prominent role for D38 (55).

In the present work we have traced the dynamics of proton release and uptake during the photocycle of BR by time-resolved step-scan FT-IR spectroscopy. As a pH-sensitive vibrational probe

we used 2-(*N*-morpholino)ethanesulfonic acid**,** MES, and its perdeuterated form, MESd_{12} (23). We exploited this technical achievement to scrutinize the current models of proton pumping by BR, in particular the proton release and uptake steps.

Results and Discussion

We prepared films of purple membranes (PMs), hydrated at 99% relative humidity. A representative absorption spectrum is shown in Fig. 2, from where we quantified the molar ratio of water/MES/BR molecules in the hydrated film to be 1570/18.1/1, using the experimentally obtained molar IR absorption spectra of BR in PMs, MES and liquid water (Fig. 2, and Experimental Section). The above spectral decomposition also provides the molar ratio of the basic and acidic forms of MES, from where the pH of the hydrated film was derived to be 6.25 (close to the pH of 6.30 of the mother solution). Figure S1 (see SI Appendix) provides a representative absorption spectrum of a film containing MESd_{12}.

The hydration level attained in our experiments, ~1,600 water molecules per BR or ~0.8 g water/g (protein + lipid) when considering the composition of the purple membrane (56), is comparable to the average composition found in cells, ~2.3 g water / g biomolecules (57). These conditions are also close to those used in molecular dynamics simulations: 12,000-6,000 water molecules per BR molecule and ~1.5-0.9 g water/g (protein + lipids) (58, 59). In contrast, experiments carried out in solution using pH-sensitive dyes commonly contained $\sim 5\times10^{6}$ water molecules per BR, or ~3,000 g water/g (protein + lipids) (9, 10, 17, 60).

The formal concentration of MES in the hydrated films, ~600 mM (~90 water molecules per buffer molecule), is $\sim 10^{4}$-fold higher than commonly used for pH-indicator dyes (9, 10, 17, 60). At this buffer concentration and pH, any excess proton at the surface of BR is expected to protonate the basic form of MES with a pseudo first-order time constant of ~100 ns, which is calculated on the basis of the second-order rate constant of 1.8×10^{7} M^{-1} s^{-1} for MES protonation (14). This response time, even if approximate, is sufficiently fast to ensure that the kinetics for proton release in BR can be traced without any significant delay.

Internal protonation changes. The photoreaction of BR was triggered by a 10 ns laser pulse of 532 nm, and time-resolved step-scan FT-IR spectroscopy was used to record transient absorption changes in the range of 2200-850 cm^{-1} (Fig. 1c). Kinetics for the protonation changes of internal groups, involved in proton transfer reactions in the photocycle of BR, can be retrieved from such data as shown before (48, 61) and briefly described below.

The rise of the positive band at ~1762 cm^{-1} reports on protonation of D85 (Fig. 1d). A shift of the carboxylic C=O stretching frequency from 1762 to 1755 cm^{-1} occurs in the M-to-N transition (62). Deprotonation of D85 is indicated by the decay of the positive band at ~1755 cm^{-1} (29, 61). D96 is protonated in the dark state of BR, with its carboxylic C=O vibration absorbing at ~1742 cm^{-1} (63). The negative band at 1739-1745 cm^{-1} in Fig. 1d is mainly caused by transient H-bonding changes of

D96, which shifts the C=O vibration to 1748 cm^{-1} in the L intermediate (64) and to 1736 cm^{-1} in the M intermediate (63). Deprotonation and reprotonation of D96 contributes to the kinetics of the negative band at ~1742 cm^{-1} in the milliseconds (Fig. 1d) although its contribution is low at pH 6.25 because the apparent pK_a of D96 in the N intermediate is ~7.1 (34, 65). Consequently, at pH 6.25 the fraction of the N intermediate with deprotonated D96 (N_1 substate) is expected to be only around 12%. Protonation of D212 from D85 gives a positive band at ~1713 cm^{-1}, although observable only at pH 4 (66). Remaining spectral changes in the carboxylic region are mostly attributable to H-bonding changes of D115 (Fig. 1d), with its carboxylic C=O vibration absorbing at ~1733 cm^{-1} in the dark-state (63). The occurrence of the very broad negative *continuum* band at frequencies above 1770 cm^{-1} in Fig. 1d is assigned to the deprotonation of the PRC (39) and decays upon dark-state recovery (38). The positive band at ~1187 cm^{-1} (Fig. 1c, arrow) can be used to monitor the deprotonation and reprotonation of the Schiff base in the 13-*cis* conformation of the retinal and, among other bands, can be used as a reporter for the formation and decay of the K, L and N intermediates (67).

Transient protonation changes of MES buffer. Among other IR features, protonation of MES buffer is characterized by a negative narrow band at 1112 cm^{-1} (23), with a moderate change in extinction coefficient of $\Delta\varepsilon$ = 210 M^{-1} cm^{-1} (see SI Appendix, Fig. S2). A small negative band is indeed observed at 1112 cm^{-1} in the light-induced IR difference spectrum of BR 370 µs after photoexcitation (Fig. 3a, blue), a time when a proton is released from the protein to the medium (7). In experiments where deuterated MESd_{12} was used (Fig. 3a, red) the negative band at 1112 cm^{-1} disappears and a positive band at 1115 cm^{-1} appears (Fig. 3a), the latter characteristic for protonation of MESd_{12} (SI Appendix, Fig. S2, and ref. (23)). Spectral changes associated with protonation of MES during the photocycle of BR become fully accessible by calculating the double difference spectrum between experiments done in MES and in MESd_{12}, after appropriate scaling to cancel the spectral response of the protein (Fig. 3b, red spectrum).

The resulting absorption changes in the double difference spectra, 2.5×10^{-4} for the most intense band at 1113 cm^{-1} (Fig. 3b, red spectrum), are 20 to 100 times smaller than typically measured with pH-indicating dyes in the visible (9, 10, 15, 60). Nevertheless, most of the bands in the double difference spectrum are clearly resolved despite their low intensity. Most importantly, the resulting spectral changes are identical to the double difference spectrum between protonation of MES and MESd_{12} induced by pH changes in the solution (Fig. 3b green spectrum), with band positions within 1 cm^{-1} agreement for nearly all bands. Given the sensitivity of molecular vibrations to their environment, this observation supports the expectation that MES molecules protonate and deprotonate in the aqueous phase, and not at the protein surface or its interior.

We monitored the protonation changes of MES, reporting on proton release and uptake from BR, from the area of the most intense negative band at 1113 cm^{-1} in the double difference spectra, as well as from the joint area of the most intense positive bands at 1093 and 1082 cm^{-1} (Fig. 3c, light blue and orange traces, respectively). Both kinetic traces are very similar as expected, although monitoring the area of the 1113 cm^{-1} band clearly gives superior signal-to-noise ratio (Fig. 3c,

compare light blue and orange traces) due to its higher intensity (SI Appendix, Fig. S2). Monitoring the area of the 1113 cm^{-1} band is also more robust to scaling errors in the subtraction of protein bands, as these contribute less than a 15% to the total area (SI Appendix, Fig. S3b).

Kinetics of proton release and uptake. Figure 4a reproduces the temporal evolution of the MES-*minus*-MESd_{12} band at 1113 cm^{-1} during the photocycle of BR. Our kinetic analysis was based on reconstructing the lifetime distributions using the maximum entropy method (68), with the benefit that the number of exponentials is not presumed a priori, as in traditional fitting approaches. Note that positive bands report on MES protonation (proton release by the protein) and negative bands on MES deprotonation (proton uptake by the protein). This convention is kept throughout the entire manuscript.

Proton release. The release of the protons to the medium detected by covalently attached dyes has been previously reported to be mono-exponential, with $\tau \approx 75$ µs (16, 17, 38). In good agreement, the analysis of the kinetics for MES protonation revealed one component for proton release with a mean time constant of 80 ± 4 µs (Fig. 4b, dashed red trace). [Confidence intervals are given here and elsewhere as plus/minus two standard deviations from Monte Carlo simulations (see Experimental Section)]. However, this component was broad and slightly asymmetric suggesting the presence of unresolved subcomponents. Indeed, increasing the resolution of the reconstructed lifetime distribution leads to the resolution of two statistically significant components for proton release with $\tau = 52 \pm 10$ µs and 150 ± 40 µs (Fig. 4b, red trace, and Fig. S4 in SI Appendix), and relative amplitudes of 67 ± 12% and 33 ± 12%, respectively.

We further confirmed that proton release is bi-exponential by reanalyzing transient absorption changes in solution from fluorescein covalently attached to K129 (see SI Appendix, Fig. S5, and ref. (10)) an amino acid located in the EC surface (Fig. 1b). Two components for proton release are clearly resolved in the corresponding lifetime distribution (Fig. 4b Insert, blue trace), with $\tau = 59 \pm 3$ µs (75 ± 4%) and 200 ± 20 µs (25 ± 4%). These results are in good agreement with those determined by MES (*vide supra*), in particular when taking into account the slight differences in temperature and pH between both experiments (see Fig. 4 legend).

Proton uptake. The analysis of the protonation kinetics of MES shows that proton uptake kinetics in BR proceeds mostly in a mono-exponential fashion. The main decay component is resolved at $\tau = 4.3 \pm 0.4$ ms (Fig. 4b, red trace). This time constant agrees with the last time constant of the photocycle obtained by global exponential fitting ($\tau = 4.4 \pm 0.1$ ms, *vide infra*), when an equilibrated mixture of the M, N and O intermediates decays to the dark state.

The lifetime distribution corresponding to protonation changes of MES also resolved a negative band at $\tau = 8 \pm 4$ µs (Fig. 4b), *i.e.*, a very early uptake of protons by BR. We can reasonably discard that such component is an artifact caused by the limited time-resolution of our FT-IR experiments because a similar negative component at $\tau = 10 \pm 2$ µs is also resolved when analyzing nanosecond-resolution fluorescein experiments (Fig. 4b, insert). Indeed, a fast response of

covalently-attached fluorescein has been observed before (38, 69), but tentatively assigned to polarity changes, an unlikely interpretation in view of its detection by MES. Thus, we conclude that some uptake of protons occur in the photocycle of BR as early as in few microseconds.

Protonation of D85 *versus* proton release. Although protonation of D85 and proton release take place at spatially distinct sites, the two reactions appear as simultaneous events under most conditions (36), the first triggering the latter by a domino effect involving fast H-bonding rearrangements and reorientation of R82 (70). Now, that it is possible to monitor both events in a single experiment, we resolved a small but clear temporal delay between protonation of D85 and proton release (Fig. 5a). For further insights we compared their lifetime distributions (Fig. 5b), displayed such that positive bands correspond to D85 protonation (blue) and to proton release (red). Protonation of D85 occurs in three phases (17, 60) with $\tau = 4 \pm 1$ µs ($10 \pm 6\%$), 38 ± 3 µs ($55 \pm 6\%$) and 115 ± 10 µs ($35 \pm 6\%$). The time constants of the second and third components are slightly faster than for proton release: 38 ± 3 µs vs 52 ± 10 µs and 115 ± 10 µs vs 150 ± 40 µs, but the deviations are modest when considering the statistical uncertainty (Fig. 5b). The most notable difference is that the first step for protonation of D85 (4 ± 1 µs) is not associated to a proton release event, but rather with a proton uptake event (8 ± 4 µs).

Kinetics of the *continuum* band *versus* proton release. If the *continuum* band is a spectral signature of the group releasing a proton to the EC medium, then its rise should display identical kinetics to proton release. But a meaningful kinetic comparison has not been possible yet (38).

We analyzed the temporal evolution of the *continuum* band by integrating the absorption changes from 1950 to 1800 cm^{-1} (Fig. 6a, black crossed dots). A significant net contribution to this area from temperature changes of water molecules during the photocycle was discarded by control experiments using the E204Q mutant (see SI Appendix, Fig. S6b), a variant that lacks absorption changes in this frequency range (38). The corresponding lifetime distribution of the *continuum* band shows two rising components with $\tau = 42 \pm 3$ µs and 150 ± 6 µs and relative amplitudes of $63 \pm 4\%$ and $37 \pm 4\%$ (Fig. 6b, red trace). These two components are basically indistinguishable at our current statistical uncertainty from those of proton release detected by MES, with $\tau = 52 \pm 10$ µs ($67 \pm 12\%$) and 150 ± 40 µs ($33 \pm 12\%$). These results are fully consistent with the PRC being the terminal group releasing a proton to the EC medium (39).

The lifetime distribution of the *continuum* band shows an additional rise with $\tau = 1.5 \pm 0.1$ ms, not associated to any proton release/uptake event (Fig. 6b, compare red and blue traces). The presence of this kinetic component has been noticed before (38). Initially, it was assigned to a LAN of water molecules assisting the proton transfer from D96 to the SB (38), but such a neutral LAN was later shown to generate a very broad absorption band above 2550 cm^{-1}, instead (71, 72). Its time evolution clearly differs from the M intermediate (compare Fig, 5a and Fig. 6a), and to less extent from the O intermediate (Fig. 6d), being most similar to that of the N intermediate (Fig. 6c). Because of the minor accumulation of the N_1 intermediate at pH 6.25, it is reasonable to associate the rise of

the second component of the *continuum* band to the formation of the N_2 intermediate (65). The accumulation of the N_2 intermediate decreases with increasing pH (34, 65). Likewise, the amplitude of the *continuum* band rising with $\tau \approx 1.5$ ms has been shown to decrease as the pH increases (73).

It is finally noted that both phases of the *continuum* band recover with $\tau = 4.5 \pm 0.1$ ms (Fig 6b). This time constant is in a closely agreement with the time constant for proton uptake, 4.3 ± 0.4 ms (Fig 4b), as well as with the recovery of the dark state: $\tau = 4.4 \pm 0.1$ ms (Fig. 7a).

Two spectrally distinct chemical groups contribute to the *continuum* band. To obtain the spectral features associated to the two kinetic components of the *continuum* band we performed global exponential fitting of the time-resolved FT-IR spectra. The derived amplitude spectra (Fig. 7a), or decay associated spectra (DAS), provide the spectral changes taking place with a specific time constant (74). The components DAS-2 and DAS-3, with $\tau = 44$ and 127 µs, respectively, correlate with the release of a proton from the protein and its acceptance by the MES buffer in the medium. Both spectra display a *continuum* band with a similar shape (Fig. 7a): the absorption changes rise in intensity from 2200 cm^{-1} to 2000 cm^{-1} and remain constant from 2000 cm^{-1} to 1800 cm^{-1}. DAS-5 with $\tau = 1.6$ ms, shows a clear *continuum* band (Fig. 7a), even though no proton is released or taken up with this time constant (Fig. 6a,b). The *continuum* band from DAS-5 continuously rises in intensity from 2200 to 1800 cm^{-1} (Fig. 7a), spectrally differing from the *continuum* band characteristic for DAS-2 and DAS-3 (Fig. 7a). The above commented spectral differences between the *continuum* bands of DAS-2 and DAS-5 are highly reproducible (Fig. 7b). We conclude that the *continuum* band observed in the DAS-5 has a molecular origin other than the PRC. Thus, the negative rise of the *continuum* band with $\tau = 1.5$ ms presumably represents the deprotonation of a newly described protonated LAN, to which we will refer as the proton uptake complex (PUC) for reasons which will be justified below.

The proton uptake complex (PUC) and reprotonation of D96. To figure out the functional role of the PUC in the proton-pumping mechanism of BR, we studied in detail the spectrum of DAS-5 (Fig. 7a). The negative band at 1187 cm^{-1}, characteristic for the C-C stretch of protonated 13-*cis* retinal, is a hallmark for the reprotonation of the SB of 13-*cis* retinal, i.e., for the formation of the N intermediate from the M intermediate (29, 67). The pH of the sample is 0.85 units below the apparent pKa of D96 in the N intermediate, favoring accumulation of the N_2 substate, with reprotonated D96 (34, 65). Consistently, a positive band at 1742 cm^{-1} from the deprotonation of D96 is hardly observable in DAS-5 (Fig. 7a) even when performing step-scan experiments at an increased resolution of 4 cm^{-1} (SI Appendix, Fig. S7). Incidentally, DAS-5 also shows retinal bands at 1506 and 1170 cm^{-1} characteristic for the formation of the O intermediate (53, 75), consistent with the known equilibration of the N and O intermediates (76). In summary, DAS-5 represents the spectral differences associated to the net formation of the N_2 and O intermediates from the M intermediate.

But how to conceive the formation of the N_2 intermediate with $\tau \approx 1.5$ ms with a reprotonated D96, when proton uptake from the medium occurs with $\tau \approx 4.5$ ms? And, if the *continuum* band with $\tau \approx 1.5$ ms reports on the deprotonation of a protonated LAN (the PUC), where is the corresponding

proton transferred to? To answer these two questions we propose that ionic D96 gets a proton in the N_1-to-N_2 transition from the PUC, not from the CP medium as currently accepted. Finally, the PUC is reprotonated in the N_2-to-O transition, taking a proton from the CP medium (Fig. 7c).

General Discussion and Conclusions

The use of buffer molecules (weak acids) to trace protonation changes in the aqueous medium during the functional mechanism of proteins solves some of the drawbacks present in the use of pH-indicating dyes (see Introduction). In particular, buffer molecules can theoretically respond to protonation changes in the medium in sub-microseconds (14), thanks to their high concentration under experimental conditions typical for IR spectroscopy. Although we have not been able to test this last prediction experimentally, we can conclude that buffer molecules can respond to protonation changes in at least 8 μs (Fig. 4b). Because pH-indicating dyes are weak acids, they are able to shuttle protons from the surface to the bulk (8). However, their typical high extinction coefficient in the visible often restricts their concentration to <100 μM (8-11), while their low concentration makes them inefficient accelerators for proton migration in practice.

The dynamics of proton release and uptake in bacteriorhodopsin are apparently more complex than previously described: proton release cannot be described by a single exponential time course as reported before (16, 17, 38), but proceeds in at least two phases with time constants of τ = 50 μs and 150 μs (Fig. 4b). Proton release lags protonation of D85 (Fig. 5) supporting photocycle models that place proton release during the transition between two M intermediates (37, 77).

Although proton uptake is predominantly mono-exponential, $\tau \approx 4.5$ ms, we resolved a very early proton uptake event taking place before 10 μs (Fig. 4b). It is conceived that this early proton uptake arises from Bohr protons. Nanosecond IR experiments (78, 79) at different pH values will be required in the future to characterize the exact timing of this early proton uptake process, as well as to understand its potential role in the photocycle and to assign the residue/s responsible for it.

Despite the current consensus that the *continuum* band in BR arises from the deprotonation of the proton release complex (PRC), it was yet to be experimentally confirmed whether proton release to the external medium tallies the rise of the *continuum* band. Due to the strict comparison of the kinetics of proton release (probed by MES buffer molecules) with the kinetics of the *continuum* band we have shown here that both processes proceed simultaneously, indeed (Fig. 6). It has been recently proposed that the PRC protonates E194, with the latter residue being the actual terminal proton release group (47). From the discrepancy between the faster component for proton release (52 $\pm$ 10 μs) and the faster rise of the *continuum* band (42 $\pm$ 3 μs), we can state that any intermediary proton acceptor/donor group in between the PRC and the external medium can hold the proton for less than 10 $\pm$ 10 μs. Given their kinetic similarity we can reasonably exclude that a metastable proton accepting group exists in between the PRC and the external medium.

Comparison of the dynamics of the *continuum* band with proton release/uptake detected by buffer molecules indicates that the *continuum* band consists of two independent kinetic (Fig. 6) and spectral (Fig. 7a,b) contributions. As elaborated above, the first contribution to the *continuum* band corresponds to deprotonation of the PRC, as shown by site-directed mutagenesis studies (39) and further confirmed herein by its temporal coincidence with proton release (Fig. 6a,b). Spectral calculations reproduce the *continuum* absorption between 2300 and 1800 cm^{-1} when, independently of molecular details, the PRC consists of a protonated LAN (41, 45, 46). Thus, the assignment of the *continuum* band to a protonated LAN at the PRC is well-supported by experiments and simulations.

We have resolved a second *continuum* band contributing to the 2300-1800 cm^{-1} range whose kinetics does not correlate with proton release (Fig. 6c). We have tentatively assigned the second component of the *continuum* band to a protonated LAN, given its spectral similarity with the *continuum* band from the PRC (Fig. 7). Further support for this assignment comes from the results that indicate the existence of an intermediary group/complex that can act as a proton donor for D96 and as a proton acceptor from the CP medium (Fig. 6 and 7): the proton uptake complex (PUC). The kinetics of the second contribution of the *continuum* band fits the expected kinetics for the PUC, consistent with its assignment to a protonated LAN. In analogy to the PRC, the protonated LAN of the PUC may involve water molecules and/or several amino acid side chains sharing a proton.

Neutral LANs also exist in BR, and their spectral contributions during the photocycle should be discussed. The pentagonal cluster (protonated SB, the charged groups D85, D212 and R82, and three water molecules) has been studied in detail by IR difference spectroscopy (80). It shows notably broad negative bands from strongly H-bonded O-H and N-H stretches, but these are centered at ≥ 2800 cm^{-1} and display a negligible contribution at frequencies below 2600 cm^{-1} (81, 82). A chain of neutral water molecules formed between the SB and D96 in the M intermediate has been associated to a broad positive band in the 2750-2550 cm^{-1} region (71, 72). However, none of these two neutral LANs contribute significantly to the 2300-1800 cm^{-1} region, which seems restricted to protonated LANs.

We anticipate that the identification of the groups comprising the PUC will require further work. Reasonable candidate residues are those that may alter the N_1/N_2 equilibrium when mutated (34), or the proton uptake kinetics (55). Among the latter, the most evident candidate is D38. Consequently, we performed preliminary time-resolved IR experiments on D38R using a tunable quantum cascade laser as an IR monochromatic source (79, 83), covering the spectral range from 1800 to 1700 cm^{-1}. Remarkably, the kinetics of the *continuum* band for the D38R variant lacks the millisecond negative rise present in WT (SI Appendix, Fig. S8), indicating that the PUC might, indeed, be disrupted upon mutation of D38. More detailed studies will be needed, though, as D38R also shows altered kinetics for the late intermediates of the photocycle (M, N and O) (55), which by itself could explain the apparent absence of the *continuum* band from the PUC.

In the current view of the proton transfer reactions in BR, D96 is reprotonated from the CP medium (Fig. 1c), either in the N-to-O transition (77) or in the N_1-to-N_2 transition (37). Instead, we

suggest that D96 accepts a proton from the PUC in the N_1-to-N_2 transition, and the PUC is reprotonated from the CP medium in the N_2-to-O transition (Fig. 7d). A piece of evidence is provided by the observation that proton uptake from the CP medium ($\tau \approx 4.5$ ms) considerably lags the formation of the N_2 intermediate, which takes place with $\tau \approx 1.5$ ms (Fig. 4b, 6c and 7a). On the other hand, the PUC deprotonates with $\tau \approx 1.5$ ms and reprotonates with $\tau \approx 4.5$ ms (Fig. 6b and 7a). Thus, our results refine the last steps of the proton pumping mechanism of BR.

The newly introduced PUC also provides a rationale for why a *continuum* band is observed under conditions that prevent deprotonation of the PRC (low pH or exchange of critical residues), although with reduced intensity and delayed kinetics (39, 73). The *continuum* band disappears completely in the E194Q and E204Q variants (38, 39), implying that these mutations impair not only the PRC but also the PUC. E194Q and E204Q variants do not only lack normal proton release but show notable alterations in the late steps of the photocycle as well (66, 84), possibly explaining why these two mutations disturb the distant PUC.

We note that our findings might also contribute to reveal the chemical nature of the PRC, an issue still not settled (46). To scrutinize different potential arrangements of the PRC, simulated vibrational spectra of the PRC have been compared to the experimental difference spectrum of the *continuum* band (41, 45, 46), extracted at 300-400 μs after photoexcitation (see Fig. 2 in ref. (39) for an example). However, at 300-400 μs not only the PRC but also the PUC contributes to the measured *continuum* band (see Fig. 6a). We have obtained the spectral signature of the *continuum* band associated to proton release by global exponential analysis (DAS-2, Fig 7b). This is the experimental spectrum that should be ideally used in future comparisons with spectral calculations of the PRC.

In closing, we have demonstrated here that the time course of proton release and uptake accompanying the photocycle of BR can be monitored by recording time-resolved vibrational changes of natural and perdeuterated buffer molecules, which work as pH-sensitive vibrational probes. As proton transfer reactions often play a critical role in protein function, similar experiments could be applicable to other proteins.

Experimental Section.

Preparation of hydrated films of bacteriorhodopsin. Purple membranes (PMs) containing either wild-type BR, E204Q, or D38R were obtained from *Halobacterium salinarum* (85-87). The PMs were washed by centrifugation and resuspended in 3 mM MES, 2 mM NaCl at pH 6.3. Around 10-20 μL of this solution was placed on top of a BaF_2 window and dried under ambient humidity, followed by rehydration in an atmosphere of 99% relative humidity, as previously described (12, 88). Equivalent films were prepared using MESd_{12} (Cambridge Isotope Laboratories Inc.) as a buffer, a molecule where all the hydrogens of MES unchangeable in water are substituted by deuterium atoms. The final molar ratio of protein, buffer and water was determined by fitting molar absorption spectra to the experimental absorption spectrum of the hydrated film (Fig. 2, and Fig. S1 in SI Appendix). We

also determined spectroscopically the pH in the hydrated film by applying the Henderson–Hasselbalch equation, using the pK_a for MES (6.06 at an ionic strength of 0.5 M and 25 °C (http://www.reachdevices.com/Protein/BiologicalBuffers.htm)) and the ratio between acidic and basic forms determined by IR absorption spectroscopy. The ionic strength of the film was calculated to be close to 1 M, minimizing complications from pH differences between the BR surface and the medium pH, that can be as high as 1.7 units at 10 mM and still near 1 unit at 100 mM (60), but only 0.2 units at 1 M ionic strength (90).

Step-scan FT-IR spectroscopy. We performed time-resolved step-scan FT-IR spectroscopy essentially as described before (12). Light-adapted BR films containing either the buffer MES or MESd_{12}, were excited by a 10 ns laser pulse (532 nm, 2 mJ/cm^2, 10 Hz) and time-resolved spectra were obtained at 6.25 µs temporal and 8 cm^{-1} spectral resolution. Some additional experiments were performed at 4 cm^{-1} spectral resolution as indicated. In each experiment, about 300-500 photoreactions were averaged at each optical retardation of the interferogram.

Maximum entropy lifetime distributions. Maximum entropy lifetime distributions were obtained from experimental time-traces as described before (91). Briefly, a maximum entropy solution vector, **h**, was obtained minimizing the function $Q(\mathbf{h}) = \chi^2(\mathbf{h}) - \alpha S(\mathbf{h})$, where S is the generalized Shannon-related entropy for solutions without sign-restriction (quantifying the simplicity of a solution), χ^2 is the chi-square function (measuring the agreement between the experimental and the predicted data), and α is a scalar which balances both terms, known as the regularization parameter. Lifetime distributions of increased detail are obtained as the value of α is reduced, given more weight to the description of the data over the simplicity of the solution. The optimum value for $\log_{10}(\alpha)$ was determined automatically using the L-curve method (92, 93). The maximum entropy lifetime distribution obtained in his way lacked enough detail for proton release/uptake measured with MES, and in this particular case the regularization value was chosen as that giving a lifetime distribution with the maximum number of statistically significant components (SI Appendix, Fig. S4). The position and area of components resolved in the lifetime distributions were characterized by their 0th (area) and 1st (mean) moments, and Monte Carlo simulations by resampling the residuals hundred times were used to estimate their confidence interval. Only bands with an area different from zero at a 96% confidence were considered to be genuine components.

Kinetics of the *continuum* band. The kinetics of the *continuum* band was obtained by integrating the absorption changes from 1950 to 1800 cm^{-1}. The baseline of the time-resolved data showed oscillations of period ~ 1 ms (see SI Appendix, Fig. S5), whose origin has been described before (94), hampering the analysis of the kinetics of the *continuum* band. We removed these oscillations by processing the spectra by SVD, discarding only 2 of the 147 SVD components (those concentrating the oscillation). Further details of this processing approach will be presented elsewhere.

Absorption coefficients of MES determined by attenuated total reflection FT-IR spectroscopy. We prepared duplicate aqueous (H_2O) solutions of MES and perdeuterated MESd_{12} at 50 mM and at 90 mM, with the pH value adjusted to 3.6 (adding HCl) and 8.5 (adding NaOH). The infrared

absorption spectrum was recorded at 25 °C and 4 cm^{-1} spectral resolution in a diamond attenuated total reflection (ATR) accessory with 9 reflections (5 of them facing the sample). We subtracted the absorption of water at the corresponding pH value to obtain the absorption spectrum of fully ionic and fully zwitterionic MES and MESd_{12} (SI Appendix, Fig. S2a). After accounting for the concentration of MES and the calculated effective penetration depth in the ATR experiment (*vide infra*), the difference molar absorption coefficient spectra were determined for protonation of MES and for protonation of MESd_{12}, and the double difference molar absorption coefficient for protonation of MES-*minus*-protonation of MESd_{12} (SI Appendix, Fig. S2b). The latter was mathematically converted to 8 cm^{-1} resolution in the Fourier domain prior to its comparison with the time-resolved double difference IR spectra between BR/MES and BR/MESd_{12} (Fig. 3b). We determined the effective penetration depth as a function of the wavenumber, $dp_{eff}(\nu)$, experimentally (SI Appendix, Fig. S9). Briefly, the absorbance of liquid water (MilliQ quality, pH 7, 25 °C) was recorded with the ATR setup (four replicates on different days), and the $dp_{eff}(\nu)$ was calculated from the concentration of water (55.34 M at 25 °C) and its published molar absorption coefficient (95).

Molar absorption coefficient of bacteriorhodopsin determined by transmission FT-IR spectroscopy. We measured the UV/Vis and IR absorption of a hydrated film of BR in PMs in the absence of buffer, previously adjusting the solution to pH 7 (SI Appendix, Fig. S9). An iris with a diameter less than 4 mm (smaller than the probing light) was placed in front of the BaF_2 window to ensure that both the UV/Vis and the infrared radiation illuminated the same area. The sandwiched sample was placed normal to the light beam. Prior to the measurements the BR film was illuminated with a LED emitting maximally at 530 nm for 1 min for light-adaptation. We estimated the IR molar absorption coefficient of light-adapted BR in the membrane plane from the extinction coefficient of the retinal chromophore: $\varepsilon_{x\text{-}y}$(570 nm) = 82,000 $M^{-1}cm^{-1}$ for. This last value was estimated from the known isotropic extinction coefficient of BR determined in solution, ε_{iso}(570 nm) = 62,700 M^{-1} cm^{-1} (96), the angle of the electronic transition moment of the retinal to the membrane normal, θ = 69° (97), and the relations for axially oriented samples: $\varepsilon_{iso} = (\varepsilon_z + 2\varepsilon_{x-y})/3$ and $(\varepsilon_z - \varepsilon_{x-y})/(\varepsilon_z + 2\varepsilon_{x-y}) = 0.5(3cos^2\theta - 1)$ (97).

.

Acknowledgments

Funding was provided by the Spanish Ministry of Economy, Industry and Competitiveness though the project BFU2016-768050-P and a Ramon y Cajal fellowship RYC-2013-13114 to V.A.L.-F., and by the German Research Foundation through the SFB-1078, projects A1 and B3 to J.H and B4 to R.S. We thank Ingrid Wallat, Elodia Serrano, and Dorothea Heinrich for skillful sample preparation of bacteriorhodopsin.

Author Information

ORCID

Victor A. Lorenz-Fonfria: 0000-0002-8859-8347

Ramona Schlesinger: 0000-0002-7716-4439
Joachim Heberle: 0000-0001-6321-2615

Author Contributions

T.L. and R.S. provided proteins. V.A.L.F. and M.S. carried out experiments. V.A.L.F. analyzed the data and drafted the manuscript. V.A.L.F., M.S., and J.H. discussed the results and wrote the manuscript. All authors read, commented and edited the final form of the manuscript.

Competing Interests: The authors declare no competing interest

References

1. Brzezinski P (2004) Redox-driven membrane-bound proton pumps. *Trends Biochem. Sci.* 29(7):380-387.
2. Lanyi JK & Pohorille A (2001) Proton pumps: mechanism of action and applications. *Trends Biotechnol.* 19(4):140-144.
3. Ataka K, Kottke T, & Heberle J (2010) Thinner, smaller, faster: IR techniques to probe the functionality of biological and biomimetic systems. *Angew. Chem. Int. Ed. Engl.* 49(32):5416-5424.
4. Gerwert K (2002) Molecular reaction mechanism of proteins monitored by time-resolved FT-IR difference spectroscopy. *Handbook of vibrational spectroscopy* eds Chalmers JM & Griffiths PR (John Wiley & Sons Ltd, Chichester).
5. Kottke T, Lorenz-Fonfria VA, & Heberle J (2017) The grateful infrared: sequential protein structural changes resolved by infrared difference spectroscopy. *J. Phys. Chem. B* 121(2):335-350.
6. Berthomieu C & Hienerwadel R (2009) Fourier transform infrared (FTIR) spectroscopy. *Photosynth. Res.* 101(2-3):157-170.
7. Heberle J (2000) Proton transfer reactions across bacteriorhodopsin and along the membrane. *Biochim. Biophys. Acta* 1458(1):135-147.
8. Drachev LA, Kaulen AD, & Skulachev VP (1984) Correlation of photochemical cycle, H^+ release and uptake, and electric events in bacteriorhodopsin. *Febs Lett.* 178(2):331-335.
9. Grzesiek S & Dencher NA (1986) Time-course and stoichiometry of light-induced proton release and uptake during the photocycle of bacteriorhodopsin. *FEBS Lett* 208(2):337-342.
10. Heberle J & Dencher NA (1992) Surface-bound optical probes monitor protein translocation and surface potential changes during the bacteriorhodopsin photocycle. *Proc. Natl. Acad. Sci. U.S.A* 89(13):5996-6000.
11. Gopta OA, Cherepanov DA, Junge W, & Mulkidjanian AY (1999) Proton transfer from the bulk to the bound ubiquinone Q_B of the reaction center in chromatophores of *Rhodobacter*

sphaeroides: retarded conveyance by neutral water. *Proc. Natl. Acad. Sci. U. S. A.* 96(23):13159-13164.

12. Lórenz-Fonfría VA & Heberle J (2014) Proton Transfer and Protein Conformation Dynamics in Photosensitive Proteins by Time-resolved Step-scan Fourier-transform Infrared Spectroscopy. *J. Vis. Exp.* 88:e51622.
13. Mulkidjanian AY, Heberle J, & Cherepanov DA (2006) Protons @ interfaces: implications for biological energy conversion. *Biochim. Biophys. Acta* 1757(8):913-930.
14. Porschke D (2002) Reaction coupling, acceptor pK, and diffusion control in light induced proton release of bacteriorhodopsin. *J. Phys. Chem. B* 106:10233-10241.
15. Alexiev U, Marti T, Heyn MP, Khorana HG, & Scherrer P (1994) Covalently bound pH-indicator dyes at selected extracellular or cytoplasmic sites in bacteriorhodopsin. 2. Rotational orientation of helices D and E and kinetic correlation between M formation and proton release in bacteriorhodopsin micelles. *Biochemistry* 33(46):13693-13699.
16. Heberle J, Riesle J, Thiedemann G, Oesterhelt D, & Dencher NA (1994) Proton migration along the membrane surface and retarded surface to bulk transfer. *Nature* 370(6488):379-382.
17. Alexiev U, Mollaaghababa R, Scherrer P, Khorana HG, & Heyn MP (1995) Rapid long-range proton diffusion along the surface of the purple membrane and delayed proton transfer into the bulk. *Proc. Natl. Acad. Sci. U. S. A.* 92(2):372-376.
18. Junge W & McLaughlin S (1987) The role of fixed and mobile buffers in the kinetics of proton movement. *Biochim. Biophys. Acta* 890(1):1-5.
19. Gutman M & Nachliel E (1997) Time-resolved dynamics of proton transfer in proteinous systems. *Annu. Rev. Phys. Chem.* 48:329-356.
20. Good NE*, et al.* (1966) Hydrogen ion buffers for biological research. *Biochemistry* 5(2):467-477.
21. Berthomieu C & Hienerwadel R (2001) Iron coordination in photosystem II: interaction between bicarbonate and the Q_B pocket studied by Fourier transform infrared spectroscopy. *Biochemistry* 40(13):4044-4052.
22. Suzuki H, Sugiura M, & Noguchi T (2008) FTIR study on the proton release pattern during water oxidation in photosystem II core complexes from *Thermosynechococcus elongatus*. in *Photosynthesis. Energy from the sun: 14th international congress on photosynthesis*, eds Allen JF, Gantt E, Golbeck JH, & Osmond B (Springer), pp 513-516.
23. Suzuki H, Sugiura M, & Noguchi T (2009) Monitoring proton release during photosynthetic water oxidation in photosystem II by means of isotope-edited infrared spectroscopy. *J. Am. Chem. Soc.* 131(22):7849-7857.
24. Lüdeke S, Mahalingam M, & Vogel R (2009) Rhodopsin activation switches in a native membrane environment. *Photochem. Photobiol.* 85(2):437-441.
25. Nakamura S & Noguchi T (2015) Infrared setection of a proton released from tyrosine Y_D

to the bulk upon its photo-oxidation in photosystem II. *Biochemistry* 54(32):5045-5053.

26. Baldassarre M & Barth A (2014) The carbonate/bicarbonate system as a pH indicator for infrared spectroscopy. *Analyst* 139(9):2167-2176.
27. Stoeckenius W (1999) Bacterial rhodopsins: evolution of a mechanistic model for the ion pumps. *Protein. Sci.* 8(2):447-459.
28. Oesterhelt D & Stoeckenius W (1973) Functions of a new photoreceptor membrane. *Proc. Natl. Acad. Sci. U. S. A.* 70(10):2853-2857.
29. Maeda A (1995) Application of FTIR spectroscopy to the structural study on the function of bacteriorhodopsin. *Isr. J. Chem.* 35:387-400.
30. Lanyi JK & Váró G (1995) The photocycles of bacteriorhodopsin. *Isr. J. Chem.* 35:365-385.
31. van Stokkum IHM & Lozier RH (2002) Target analysis of the bacteriorhodopsin photocycle using a spectrotemporal model. *J. Phys. Chem. B* 106(3477-3485).
32. Lórenz-Fonfría VA & Kandori H (2009) Spectroscopic and kinetic evidence on how bacteriorhodopsin accomplishes vectorial proton transport under functional conditions. *J. Am. Chem. Soc.* 131(16):5891-5901.
33. Váró G & Lanyi JK (1991) Kinetic and spectroscopic evidence for an irreversible step between deprotonation and reprotonation of the Schiff base in the bacteriorhodopsin photocycle. *Biochemistry* 30(20):5008-5015.
34. Dioumaev AK, Brown LS, Needleman R, & Lanyi JK (2001) Coupling of the reisomerization of the retinal, proton uptake, and reprotonation of Asp-96 in the N photointermediate of bacteriorhodopsin. *Biochemistry* 40(38):11308-11317.
35. Ames JB & Mathies RA (1990) The role of back-reactions and proton uptake during the N →O transition in bacteriorhodopsin's photocycle: a kinetic resonance Raman study. *Biochemistry* 29(31):7181-7190.
36. Lanyi JK (2004) Bacteriorhodopsin. *Annu. Rev. Physiol.* 66:665-688.
37. Lanyi JK (2006) Proton transfers in the bacteriorhodopsin photocycle. *Biochim. Biophys. Acta* 1757(8):1012-1018.
38. Rammelsberg R, Huhn G, Lübben M, & Gerwert K (1998) Bacteriorhodopsin's intramolecular proton-release pathway consists of a hydrogen-bonded network. *Biochemistry* 37(14):5001-5009.
39. Garczarek F, Brown LS, Lanyi JK, & Gerwert K (2005) Proton binding within a membrane protein by a protonated water cluster. *Proc. Natl. Acad. Sci. U. S. A.* 102(10):3633-3638.
40. Heberle J (2004) A local area network of protonated water molecules. *Biophys. J.* 87(4):2105-2106.
41. Mathias G & Marx D (2007) Structures and spectral signatures of protonated water networks in bacteriorhodopsin. *Proc. Natl. Acad. Sci. U S A* 104(17):6980-6985.
42. Janoschek R, Weideman EG, Zundel G, & Pfeiffer H (1972) Extremely high polarizability of hydrogen-bonds. *J. Am. Chem. Soc.* 94(7):2387-&.

43. Kalish NB, Shandalov E, Kharlanov V, Pines D, & Pines E (2011) Apparent stoichiometry of water in proton hydration and proton dehydration reactions in CH3CN/H2O solutions. *J. Phys. Chem. A* 115(16):4063-4075.
44. Dahms F*, et al.* (2016) The Hydrated Excess Proton in the Zundel Cation $H_5O_2^+$: The Role of Ultrafast Solvent Fluctuations. *Angew. Chem. Int. Ed. Engl.* 55(36):10600-10605.
45. Phatak P, Ghosh N, Yu H, Cui Q, & Elstner M (2008) Amino acids with an intermolecular proton bond as proton storage site in bacteriorhodopsin. *Proc. Natl. Acad. Sci. U.S.A.* 105(50):19672-19677.
46. Wolf S, Freier E, & Gerwert K (2014) A delocalized proton-binding site within a membrane protein. *Biophys. J.* 107(1):174-184.
47. Wolf S, Freier E, Potschies M, Hofmann E, & Gerwert K (2010) Directional proton transfer in membrane proteins achieved through protonated protein-bound water molecules: a proton diode. *Angew. Chem. Int. Ed. Engl.* 49(38):6889-6893.
48. Souvignier G & Gerwert K (1992) Proton uptake mechanism of bacteriorhodopsin as determined by time-resolved stroboscopic-FTIR-spectroscopy. *Biophys. J.* 63:1393-1405.
49. Lozier RH, Bogomolni RA, & Stoeckenius W (1975) Bacteriorhodopsin: a light-driven proton pump in *Halobacterium Halobium*. *Biophys. J.* 15(9):955-962.
50. Dencher N & Wilms M (1975) Flash photometric experiments on the photochemical cycle of bacteriorhodopsin. *Biophys. Struct. Mech.* 1(3):259-271.
51. Stoeckenius W (1985) The rhodopsin-like pigments of halobacteria: light-energy and signal transducers in an archaebacterium. *Trends Biochem. Sci.* 10(12):483-486.
52. Otto H*, et al.* (1989) Aspartic acid-96 is the internal proton donor in the reprotonation of the Schiff base of bacteriorhodopsin. *Proc. Natl. Acad. Sci. U. S. A.* 86(23):9228-9232.
53. Heßling B, Souvignier G, & Gerwert K (1993) A model-independent approach to assigning bacteriorhodopsin's intramolecular reactions to photocycle intermediates. *Biophys. J.* 65(5):1929-1941.
54. Checover S, Nachliel E, Dencher NA, & Gutman M (1997) Mechanism of proton entry into the cytoplasmic section of the proton-conducting channel of bacteriorhodopsin. *Biochemistry* 36(45):13919-13928.
55. Riesle J, Oesterhelt D, Dencher NA, & Heberle J (1996) D38 is an essential part of the proton translocation pathway in bacteriorhodopsin. *Biochemistry* 35(21):6635-6643.
56. Henderson R (1977) The purple membrane from *Halobacterium halobium*. *Annu. Rev. Biophys. Bioeng.* 6:87-109.
57. Voet D & Voet JG (2011) *Biochemistry* (John Wiley & Sons, Inc.) 4th Ed.
58. Kandt C, Schlitter J, & Gerwert K (2004) Dynamics of water molecules in the bacteriorhodopsin trimer in explicit lipid/water environment. *Biophys. J.* 86(2):705-717.
59. Del Val C, Bondar L, & Bondar AN (2014) Coupling between inter-helical hydrogen bonding and water dynamics in a proton transporter. *J. Struct. Biol.* 186(1):95-111.

60. Cao Y, *et al.* (1995) Relationship of proton release at the extracellular surface to deprotonation of the schiff base in the bacteriorhodopsin photocycle. *Biophys. J.* 68(4):1518-1530.
61. Lórenz-Fonfría VA, Kandori H, & Padrós E (2011) Probing specific molecular processes and intermediates by time-resolved Fourier transform infrared spectroscopy: application to the bacteriorhodopsin photocycle. *J. Phys. Chem. B* 115(24):7972-7985.
62. Braiman MS, Bousche O, & Rothschild KJ (1991) Protein dynamics in the bacteriorhodopsin photocycle: submillisecond Fourier transform infrared spectra of the L, M, and N photointermediates. *Proc. Natl. Acad. Sci. U. S. A.* 88(6):2388-2392.
63. Sasaki J, Lanyi JK, Needleman R, Yoshizawa T, & Maeda A (1994) Complete identification of C=O stretching vibrational bands of protonated aspartic acid residues in the difference infrared spectra of M and N intermediates versus bacteriorhodopsin. *Biochemistry* 33(11):3178-3184.
64. Gerwert K, Hess B, Soppa J, & Oesterhelt D (1989) Role of aspartate-96 in proton translocation by bacteriorhodopsin. *Proc. Natl. Acad. Sci. U. S. A.* 86(13):4943-4947.
65. Zscherp C, Schlesinger R, Tittor J, Oesterhelt D, & Heberle J (1999) *In situ* determination of transient pK_a changes of internal amino acids of bacteriorhodopsin by using time-resolved attenuated total reflection Fourier-transform infrared spectroscopy. *Proc. Natl. Acad. Sci. U. S. A.* 96(10):5498-5503.
66. Zscherp C, Schlesinger R, & Heberle J (2001) Time-resolved FT-IR spectroscopic investigation of the pH-dependent proton transfer reactions in the E194Q mutant of bacteriorhodopsin. *Biochem. Biophys. Res. Commun.* 283(1):57-63.
67. Gerwert K, Souvignier G, & Hess B (1990) Simultaneous monitoring of light-induced changes in protein side-group protonation, chromophore isomerization, and backbone motion of bacteriorhodopsin by time-resolved Fourier-transform infrared spectroscopy. *Proc. Natl. Acad. Sci. U. S. A.* 87(24):9774-9778.
68. Brochon JC (1994) Maximum entropy method of data analysis in time-resolved spectroscopy. *Methods Enzymol.* 240:262-311.
69. Heberle J & Dencher NA (1990) Bacteriorhodopsin in ice. Accelerated proton transfer from the purple membrane surface. *FEBS Lett.* 277(1-2):277-280.
70. Clemens M, Phatak P, Cui Q, Bondar AN, & Elstner M (2011) Role of Arg82 in the early steps of the bacteriorhodopsin proton-pumping cycle. *J. Phys. Chem. B* 115(21):7129-7135.
71. Freier E, Wolf S, & Gerwert K (2011) Proton transfer via a transient linear water-molecule chain in a membrane protein. *Proc. Natl. Acad. Sci. U. S. A.* 108(28):11435-11439.
72. Wolf S, Freier E, Cui Q, & Gerwert K (2014) Infrared spectral marker bands characterizing a transient water wire inside a hydrophobic membrane protein. *J. Chem. Phys.* 141(22):22D524.
73. Wolf S, Freier E, & Gerwert K (2008) How does a membrane protein achieve a vectorial

proton transfer via water molecules? *Chemphyschem* 9(18):2772-2778.

74. van Stokkum IH, Larsen DS, & van Grondelle R (2004) Global and target analysis of time-resolved spectra. *Biochim. Biophys. Acta* 1657(2-3):82-104.
75. Zscherp C & Heberle J (1997) Infrared difference spectra of the intermediates L, M, N, and O of the bacteriorhodopsin photoreaction obtained by time-resolved attenuated total reflection spectroscopy. *J. Phys. Chem. B* 101:10542-10547.
76. Chernavskii DS*, et al.* (1989) Kinetic model of bacteriorhodopsin photocycle: pathway from M state to bR. *Photochem. Photobiol.* 49(5):649-653.
77. Balashov SP (2000) Protonation reactions and their coupling in bacteriorhodopsin. *Biochim. Biophys. Acta.* 1460(1):75-94.
78. Resler T, Schultz BJ, Lórenz-Fonfría VA, Schlesinger R, & Heberle J (2015) Kinetic and vibrational isotope effects of proton transfer reactions in channelrhodopsin-2. *Biophys. J.* 109(2):287-297.
79. Lórenz-Fonfría VA*, et al.* (2015) Pre-gating conformational changes in the ChETA variant of channelrhodopsin-2 monitored by nanosecond IR spectroscopy. *J. Am. Chem. Soc.* 137(5):1850-1861.
80. Shibata M & Kandori H (2005) FTIR studies of internal water molecules in the Schiff base region of bacteriorhodopsin. *Biochemistry* 44(20):7406-7413.
81. Baer M*, et al.* (2008) Spectral Signatures of the Pentagonal Water Cluster in Bacteriorhodopsin. *Chemphyschem* 9(18):2703-2707.
82. Kandori H, Kinoshita N, Shichida Y, & Maeda A (1998) Protein structural changes in bacteriorhodopsin upon photoisomerization as revealed by polarized FTIR spectroscopy. *J. Phys. Chem. B* 102:7899-7905.
83. Schultz BJ, Mohrmann H, Lorenz-Fonfria VA, & Heberle J (2017) Protein dynamics observed by tunable mid-IR quantum cascade lasers across the time range from 10 ns to 1 s. *Spectrochim. Acta A Mol. Biomol. Spectrosc.*
84. Dioumaev AK, Brown LS, Needleman R, & Lanyi JK (1999) Fourier transform infrared spectra of a late intermediate of the bacteriorhodopsin photocycle suggest transient protonation of Asp-212. *Biochemistry* 38(31):10070-10078.
85. Oesterhelt D & Stoeckenius W (1974) Isolation of the cell membrane of Halobacterium halobium and its fractionation into red and purple membrane. *Methods Enzymol* 31(Pt A):667-678.
86. Gordeliy VI, Schlesinger R, Efremov R, Buldt G, & Heberle J (2003) Crystallization in lipidic cubic phases: a case study with bacteriorhodopsin. *Methods Mol. Biol.* 228:305-316.
87. Sanz C*, et al.* (1999) Opening the Schiff base moiety of bacteriorhodopsin by mutation of the four extracellular Glu side chains. *FEBS Lett.* 456(1):191-195.
88. Noguchi T & Sugiura M (2002) Flash-induced FTIR difference spectra of the water oxidizing complex in moderately hydrated photosystem II core films: effect of hydration

extent on S-state transitions. *Biochemistry* 41(7):2322-2330.

89. Szundi I & Stoeckenius W (1989) Surface pH controls purple-to-blue transition of bacteriorhodopsin. A theoretical model of purple membrane surface. *Biophys. J.* 56(2):369-383.

90. Alexiev U, Marti T, Heyn MP, Khorana HG, & Scherrer P (1994) Surface charge of bacteriorhodopsin detected with covalently bound pH indicators at selected extracellular and cytoplasmic sites. *Biochemistry* 33(1):298-306.

91. Lorenz-Fonfria VA & Kandori H (2006) Transformation of time-resolved spectra to lifetime-resolved spectra by maximum entropy inversion of the Laplace transform. *Appl. Spectrosc.* 60:407-417.

92. Hansen PC (1992) Analysis of discrete ill-posed problems by means of the L-curve. *SIAM review* 34:561-580.

93. Lórenz-Fonfría VA & Kandori H (2007) Bayesian maximum entropy (2D) lifetime distribution reconstruction from time-resolved spectroscopic data. *Appl. Spectrosc.* 61(4):428-443.

94. Rödig C & Siebert F (2002) Instrumental aspects of time-resolved spectra generated using step-scan interferometers. *Handbook of vibrational spectroscopy*, eds Chalmers JM & Griffiths PG (John Wiley & Sons, Chichester).

95. Bertie JE & Lan ZD (1996) Infrared intensities of liquids XX: the intensity of the OH stretching band of liquid water revisited, and the best current values of the optical constants of $H_2O(l)$ at 25 °C between 15,000 and 1 cm^{-1}. *Appl. Spectrosc.* 50(8):1047-1057.

96. Rehorek M & Heyn MP (1979) Binding of all-*trans*-retinal to the purple membrane. Evidence for cooperativity and determination of the extinction coefficient. *Biochemistry* 18(22):4977-4983.

97. Heyn MP, Borucki B, & Otto H (2000) Chromophore reorientation during the photocycle of bacteriorhodopsin: experimental methods and functional significance. *Biochim. Biophys. Acta* 1460(1):60-74.

98. Luecke H, Schobert B, Richter HT, Cartailler JP, & Lanyi JK (1999) Structure of bacteriorhodopsin at 1.55 Å resolution. *J. Mol. Biol.* 291(4):899-911.

99. Kauppinen JK, Moffatt DJ, Mantsch HH, & Cameron DG (1981) Fourier self-deconvolution: a method for resolving intrinsically overlapped bands. *Appl. Spectrosc.* 35:271-276.

Figure Legends

Figure 1. Proton transfer reactions during the photoreaction of BR. (a) Basic photocycle scheme, and (b) proton transfer steps overlaid with the dark-state structure (pdb 1c3w, ref. (98)): i) from the protonated Schiff base (SB) of the retinal chromophore to ionic D85; ii) from the proton release complex (PRC) to the extracellular (EC) medium; iii) from D96 to the retinal SB; iv) from the cytoplasmic (CP) medium to ionic D96; and finally v) from D85 to the PRC via D212 (66, 84), (c) Time-resolved step-scan FT-IR difference spectra after 10 ns laser pulse excitation. (d) Expanded absorption changes in the 2000-1700 cm^{-1} the region, with contributions from the C=O stretch of D85, D96 and D115, as well as from the *continuum* band, assigned to the PRC.

Figure 2. Spectral decomposition of the chemical components in a hydrated film of BR in PMs. FT-IR absorption spectrum of the film (top, black trace) and of its second derivative (bottom, black trace). Fitted spectra (dashed red traces) were obtained by adding the molar absorption spectra of water (light blue traces), BR in PMs (light purple traces), and the acidic and basic forms of MES (red and blue traces) after appropriate scaling. The scaling factors needed for a successful fit of the experimental spectra provided the moles per unit area for the different chemical species. Minor absorption from the BaF_2 windows was subtracted.

Figure 3. Detection of proton release and uptake kinetics in the photocycle of BR from protonation changes of the MES buffer. (a) FT-IR difference spectrum taken at 370 μs after photoexcitation of BR, using either MES (blue spectrum) or MESd_{12} (red spectrum) as buffer. (b) Subtraction of the spectra in (a) cancels protein signals (red spectrum). The scaling factor of 1.04 used in (b) was determined with objectivity thanks to the broad spectral range covered by FT-IR spectroscopy (see SI Appendix, Fig. S3a). The resulting spectrum is identical to pH-induced differences of MES minus MESd_{12} in solution (green spectrum). (c) Dynamics of protonation changes of MES using the area of different bands as indicated. These two areas were measured with an internal baseline (see the shaded blue and orange band areas in (b)), making the obtained kinetic traces insensitive to drifts in the spectral zero line (61).

Figure 4. Lifetime distribution analysis of proton release and uptake in the photocycle of BR (25 ^{o}C, pH 6.25 and 1 M NaCl). (a) Kinetics (open gray circles) and fit (continuous line) for protonation changes of MES monitored by the area of the band at 1113 cm^{-1} in the BR/MES-minus-BR/MESd_{12} double difference spectra. The residual between the data and the fit is shown as a gray continuous line. (b) Lifetime distributions for protonation changes of MES (continuous and dashed red traces). Positive bands correspond to proton release and negative bands to proton uptake. (Inset) Lifetime distribution for protonation kinetics detected by the absorption changes of fluorescein (22 ^{o}C, pH 7.5 and 400 mM NaCl) at 489 nm (blue trace). The lifetime distribution for protonation kinetics detected by MES is also depicted (red trace) for comparison. Bands marked with an asterisk are statistically insignificant at a 96% confidence interval.

Figure 5. Comparison of (a) the kinetics and (b) the lifetime distribution for protonation changes of D85 (blue trace) and proton release/uptake (red trace), after appropriate scaling. The kinetics of the C=O stretching of protonated D85 was monitored from the area between 1771 and 1750 cm^{-1}, using an internal baseline that minimizes cross-contributions from nearby bands (61).

Figure 6. Lifetime distribution analysis of the rise and decay of the *continuum* band. (a) The kinetics of the *continuum* band, monitored by the area between 1950 and 1800 cm^{-1} (gray circles), fitted by the maximum entropy method (continuous blue trace), and decomposed into two kinetic components: the proton release complex, PRC (blue dashed lines), and the proton uptake complex, PUC (green dashed lines). (b) Lifetime distribution for the *continuum* band (blue trace). The kinetics and lifetime distribution for proton release and uptake (measured with MES) are shown, after scaling, for comparison purposes (red traces in (a) and (b)). (c) The time-evolution of the N intermediate was traced using the absorption changes of the positive retinal C-C stretching band at 1187 cm^{-1} (29, 67), after band narrowing by Fourier self-deconvolution (99) to reduce contributions from negative overlapping bands (black trace), and compared with the expected kinetics for the PUC (green dashed trace). (d) The time-evolution of the O intermediate was probed with the positive band at 1505 cm^{-1} (black trace), coming from the in phase C=C stretching of the retinal (75), and compared with the expected kinetics for the PUC (green dashed trace).

Figure 7. Spectral signatures for the PRC and the PUC, and revised model for proton transfer reactions in BR. (a) Decay associated spectra (DAS) obtained from global exponential fitting analysis of time-resolved FT-IR experiments at 8 cm^{-1} resolution using MES and MESd_{12} as buffer (blue and red continuous lines, respectively). The region between 2150 and 1800 cm^{-1} is 20-fold magnified (dashed lines). The DAS with τ = 4.4 ms is scaled by 0.5 for displaying purposes. (b) DAS-2 and DAS-5 for five independent experiments, including their average (back line). The asterisk marks a band originated from MESd_{12}. (c) Extended photocycle scheme of BR, integrated into the dark-state structure (98). The precise chemical nature and location of the proton uptake complex (PUC) remains elusive, but its deprotonation is characterized by the *continuum* band from DAS-5 (see (b)).

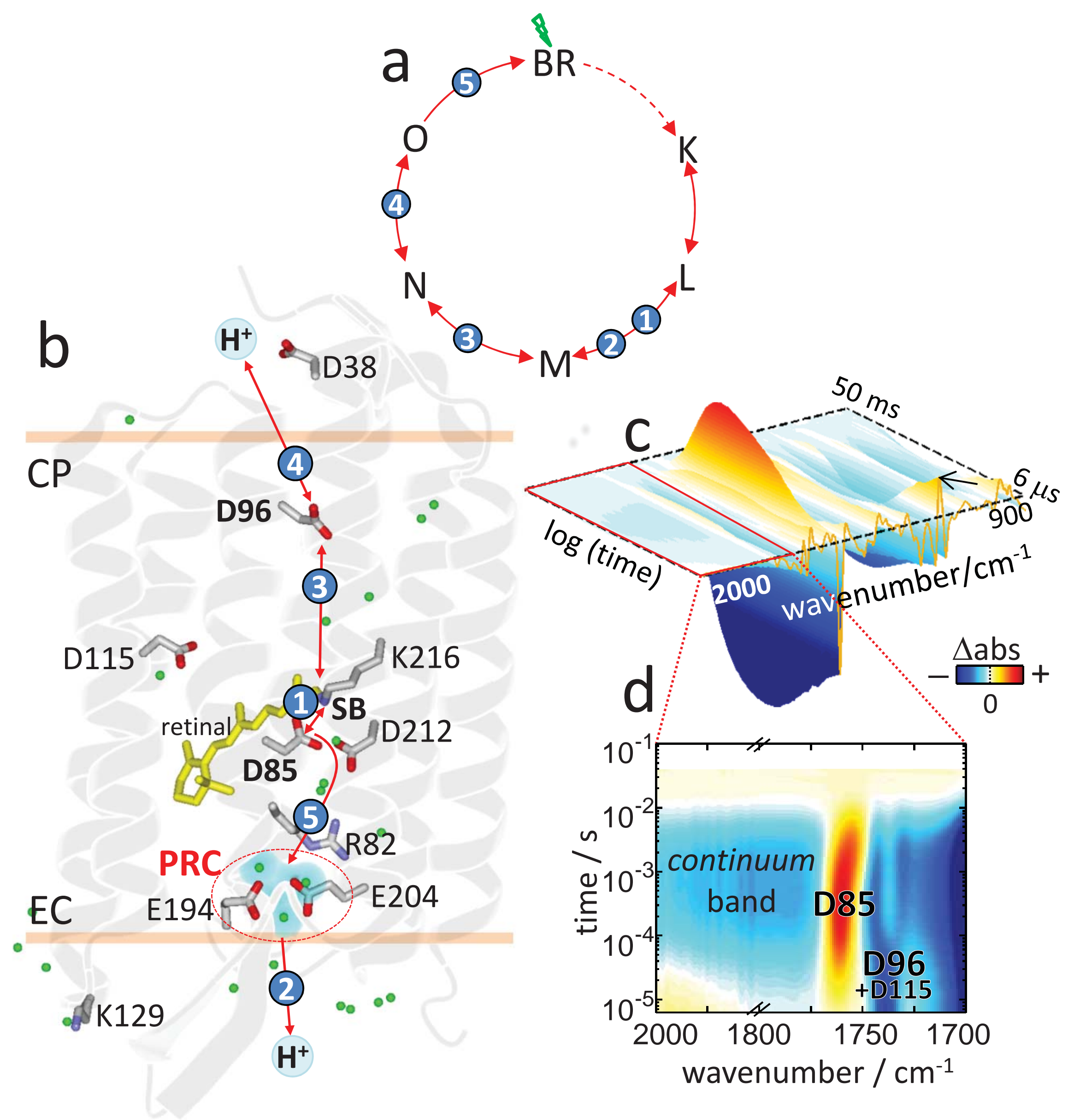
a
BR
K
L
M
N
O
1
2
3
4
5
b
H+
D38
CP
D96
D115
K216
SB
retinal
D212
D85
R82
PRC
E194
E204
EC
K129
H+
c
50 ms
6 µs
900
log (time)
2000
wavenumber/cm-1
Δabs
–
+
0
d
continuum
band
D85
D96
+D115
time / s
wavenumber / cm-1
2000
1800
1750
1700

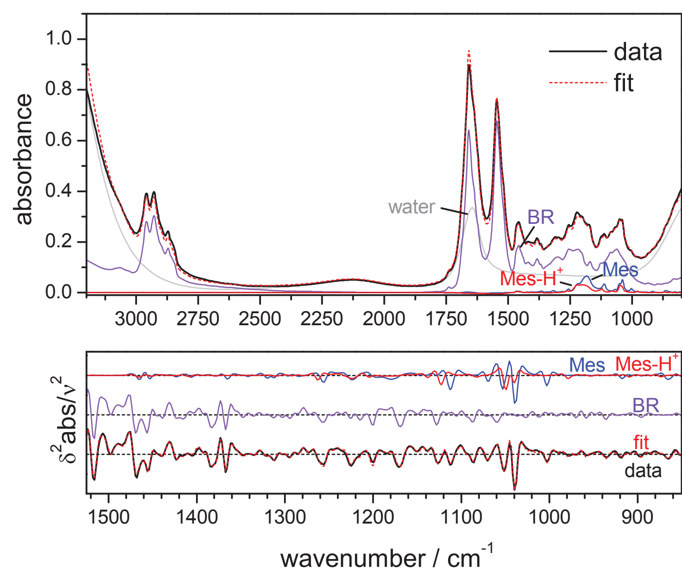
data
fit
absorbance
water
BR
Mes-H+
Mes
1.0
0.8
0.6
0.4
0.2
0.0
3000
2750
2500
2250
2000
1750
1500
1250
1000
Mes
Mes-H+
BR
fit
data
δ2abs/ν2
1500
1400
1300
1200
1100
1000
900
wavenumber / cm-1

a

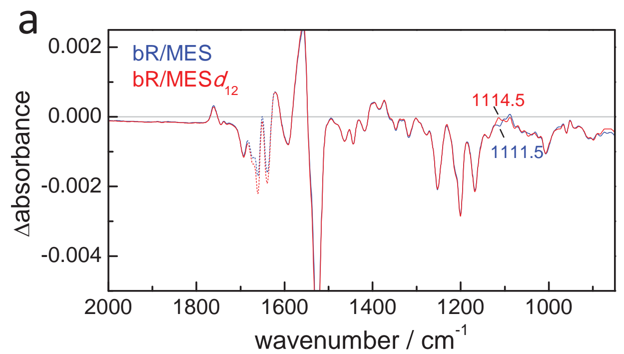

b

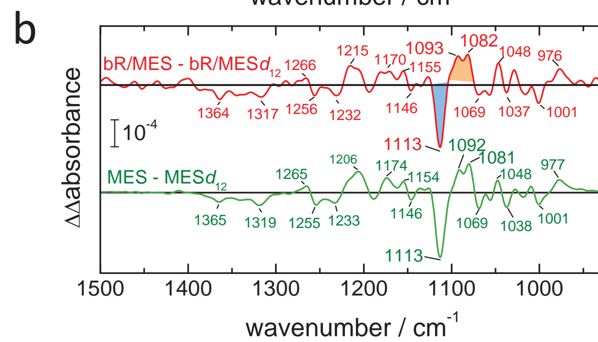

c

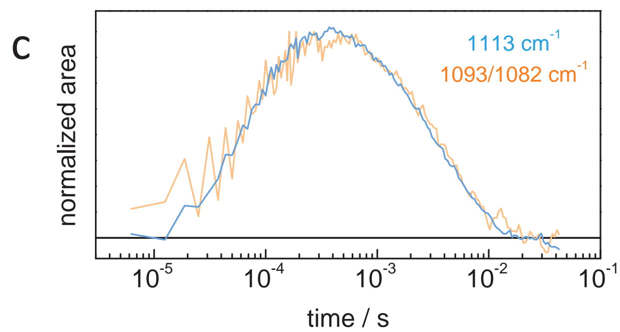

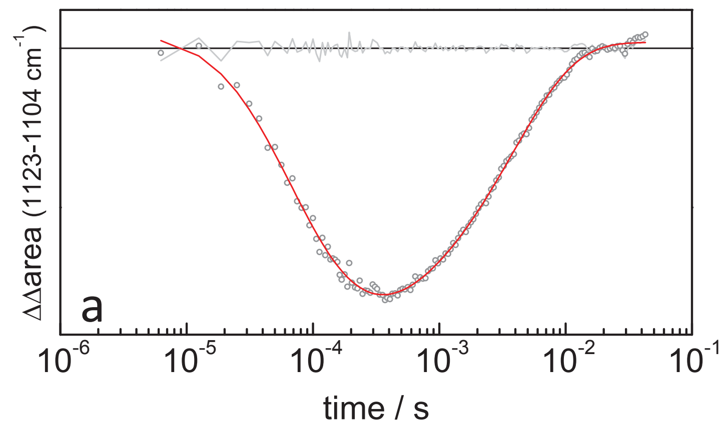

ΔΔarea (1123-1104 cm⁻¹)
a
10-6
10-5
10-4
10-3
10-2
10-1
time / s

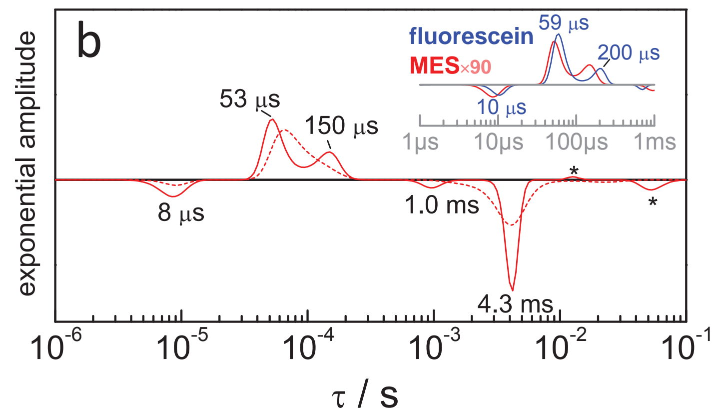

b
exponential amplitude
fluorescein
MES×90
59 μs
200 μs
10 μs
1μs
10μs
100μs
1ms
53 μs
150 μs
8 μs
1.0 ms
4.3 ms
*
*
10-6
10-5
10-4
10-3
10-2
10-1
τ / s

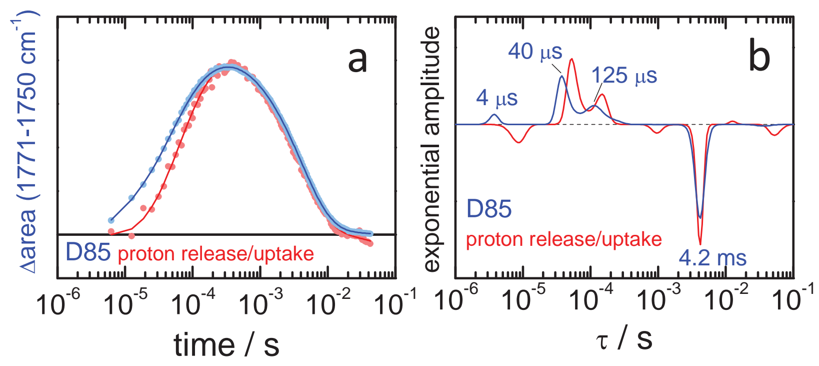

a
Δarea (1771-1750 cm-1)
D85
proton release/uptake
time / s
b
exponential amplitude
4 μs
40 μs
125 μs
4.2 ms
D85
proton release/uptake
τ / s

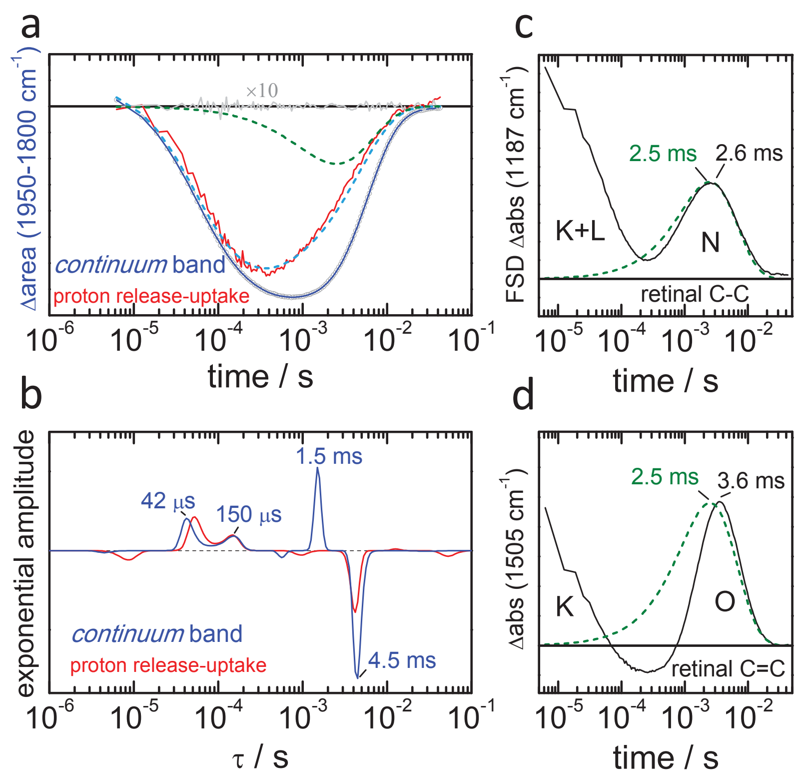
a
Δarea (1950-1800 cm^{-1})
×10
continuum band
proton release-uptake
time / s
b
exponential amplitude
42 μs
150 μs
1.5 ms
4.5 ms
continuum band
proton release-uptake
τ / s
c
FSD Δabs (1187 cm^{-1})
2.5 ms
2.6 ms
K+L
N
retinal C-C
time / s
d
Δabs (1505 cm^{-1})
2.5 ms
3.6 ms
K
O
retinal C=C
time / s

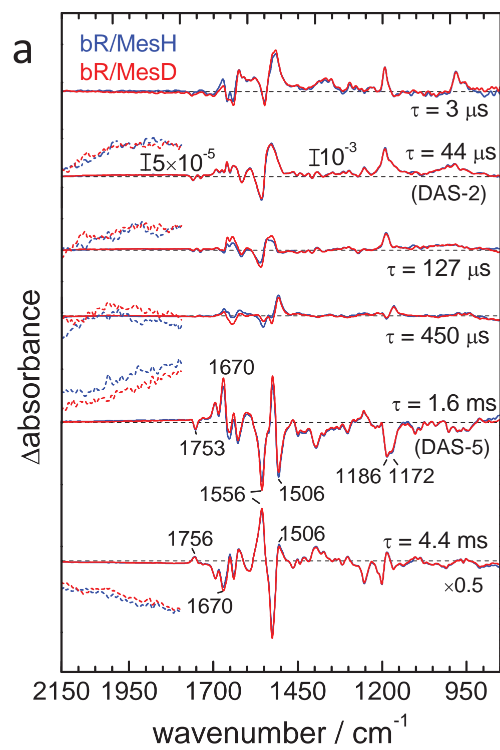
a
bR/MesH
bR/MesD
τ = 3 μs
τ = 44 μs
(DAS-2)
5×10^-5
10^-3
τ = 127 μs
τ = 450 μs
τ = 1.6 ms
(DAS-5)
1670
1753
1556
1506
1186
1172
τ = 4.4 ms
1756
1506
1670
×0.5
Δabsorbance
2150 1950 1700 1450 1200 950
wavenumber / cm^-1

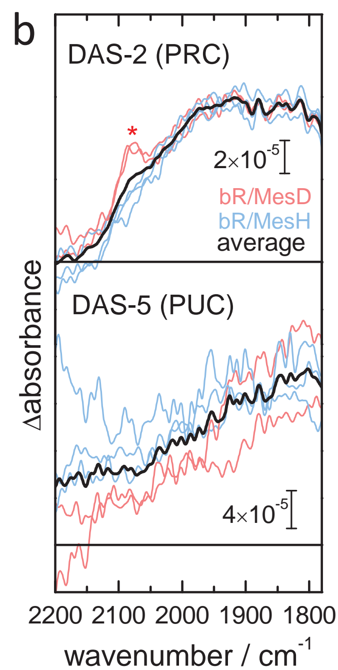
b
DAS-2 (PRC)
*
2×10^-5
bR/MesD
bR/MesH
average
DAS-5 (PUC)
4×10^-5
Δabsorbance
2200 2100 2000 1900 1800
wavenumber / cm^-1

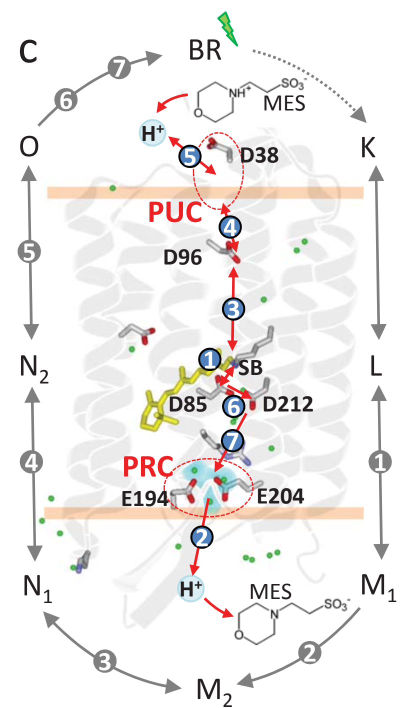
c
BR
MES
K
O
H+
D38
PUC
D96
SB
D85
D212
PRC
E194
E204
H+
MES
N2
L
N1
M1
M2